Biosensors and Bioelectronics 50 (2013) 345–350

Contents lists available at SciVerse ScienceDirect

Biosensors and Bioelectronics

journal homepage: www.elsevier.com/locate/bios

A carbon nanotube metal semiconductor field effect transistor-based biosensor for detection of amyloid-beta in human serum

Jeseung Oh [a], Gu Yoo [c], Young Wook Chang [a], Hyung Joon Kim [a], Joachim Jose [d], Eosu Kim [e], Jae-Chul Pyun [c], Kyung-Hwa Yoo [a,b,*]

[a] Nanomedical Graduate Program, Yonsei University, Seoul 120-749, Republic of Korea
[b] Department of Physics, Yonsei University, Seoul, 120-749, Republic of Korea
[c] Department of Materials Science and Engineering, Yonsei University, Seoul, 120-749, Republic of Korea
[d] Institute of Pharmaceutical and Medical Chemistry, University of Muenster, Muenster, Germany
[e] Department of Psychiatry, Institute of Behavioral Science in Medicine, Yonsei University College of Medicine, Seoul 120-749, Republic of Korea

ARTICLE INFO

Article history:
Received 14 May 2013
Received in revised form
3 July 2013
Accepted 4 July 2013
Available online 11 July 2013

Keywords:
Carbon nanotube
Metal semiconductor field effect transistor
Biosensor
E. coli outer membrane with autodisplayed Z-domain
Amyloid-β
Alzheimer's disease
Human serum

ABSTRACT

We have developed a carbon nanotube (CNT) film-based biosensor with a metal semiconductor field effect transistor structure (MESFET). A gold top gate was deposited on the middle of the CNT channel and probe antibodies were immobilized on the gold top gate with an antibody-binding protein, protein G or *Escherichia coli* outer membrane (OM) with autodisplayed Z-domains of protein A. These CNT-MESFET biosensors exhibited a higher sensitivity than the CNT-FET biosensor with probe antibodies immobilized using a chemical linker, since the orientation of immobilized antibodies was controlled by the antibody-binding proteins. In addition, nonspecific binding was effectively inhibited by *E. coli* OM. Using the CNT-MESFET biosensors with *E. coli* OM containing Z domain, we detected amyloid-β (Aβ) in human serum, one of the biomarkers for early diagnosis of Alzheimer's disease. Aβ at the level of 1 pg/mL in human serum could be measured in real-time and without labeling, which was lower than a limit of detection for plasma Aβ using an enzyme-linked immune sorbent assay. These results suggested that our CNT-MESFET biosensors might be applicable for an early diagnosis of Alzheimer's disease.

1. Introduction

Immunoaffinity (IA) biosensors based on a carbon nanotube (CNT) with a field effect transistor (FET) structure have been extensively studied for their merits (Allen et al., 2007; Li et al., 2005; Maehashi et al., 2007; Hu et al., 2011), which include label-free detection, real-time monitoring, ultra-sensitivity, and simplicity of apparatus. Target analytes are detected by measuring a change in the electrical conductance of CNT-FET that is caused by binding of target analytes to antigen-binding sites (Fab regions) of antibodies immobilized on the surface of CNTs (Fig. S1). For most CNT-FET IA biosensors, probe antibodies have been immobilized on the CNT surface using a chemical linker, such as pyrenebutyric acid *N*-hydroxylsuccinimide ester (Chen et al., 2001; Oh et al., 2009). However, this linker makes the antibodies bind onto the CNT surface with a random orientation, so that only a small portion of antibodies are immobilized with a proper orientation for binding analytes. Therefore, improved sensor performance may be achieved by increasing the density of antibodies that are immobilized on the sensor surface via the Fc region of antibodies (Fig. S1).

We have developed a semiconducting CNT film-based biosensor with a metal semiconductor field effect transistor structure (CNT-MESFET, Fig. 1(a)). A gold (Au) strip is deposited on the middle of the CNT film channel. Then, a Schottky barrier forms at an interface between the Au strip and the CNT (Oh et al., 2010). For this CNT-MESFET biosensor, probe antibodies can be immobilized on the Au top gate with an antibody-binding protein, such as protein G or protein A. The antibody-binding protein has a high affinity toward the Fc region of antibodies, so the antibodies are immobilized on the Au surface without the involvement of the Fab regions, leading to an increase in the density of probe antibodies with the proper orientation for binding analytes.

Here, we report the fabrication of the CNT-MESFET biosensors using semiconducting CNT films to minimize device-to-device variation (Wang et al., 2009). The fabricated devices exhibited a narrow distribution in the threshold voltage (V_{th}) and the on/off ratio, offering reproducible sensor performance. Probe antibodies were immobilized on the Au top gate of CNT-MESFET using protein G or *E. coli* outer membrane (OM) with autodisplayed Z-domains

* Corresponding author at: Department of Physics, Yonsei University, Seoul 120-749, Republic of Korea. Tel.: +82 2 2123 3887; fax: +82 2 312 7090.
E-mail address: khyoo@yonsei.ac.kr (K.-H. Yoo).

0956-5663/$ - see front matter © 2013 Elsevier B.V. All rights reserved.
http://dx.doi.org/10.1016/j.bios.2013.07.004

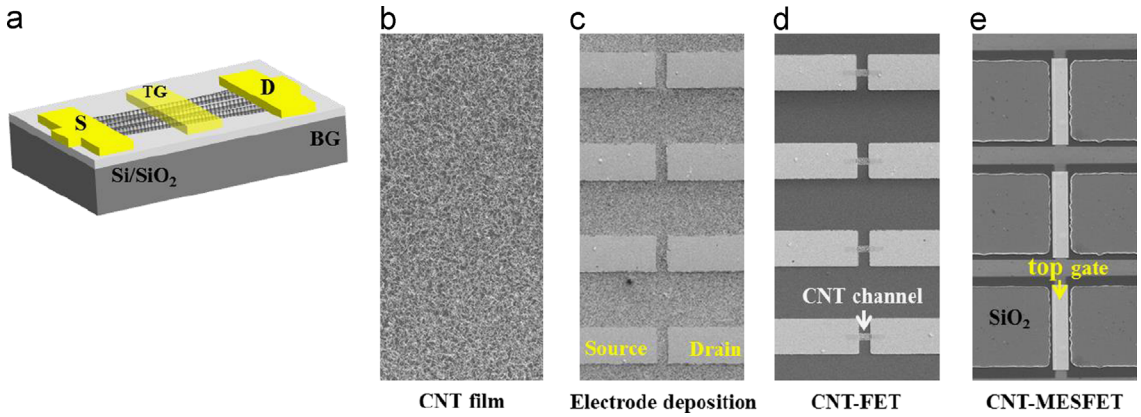

Fig. 1. (a) Schematic diagram of a CNT-MESFET device. (b–e) Fabrication procedure of the CNT-MESFET devices.

of protein A. When target analytes bound to the Au surface with immobilized antibodies, the conductance of the CNT channel changed owing to a potential change of the CNT channel covered with the Au top gate, allowing us to detect target analytes in real-time (Oh et al., 2010). The sensitivity of the CNT-MESFET biosensor was compared with that of CNT-FET biosensors using horseradish peroxidase (HRP) as a model target analyte. Indeed, the CNT-MESFET biosensor with antibody-binding proteins exhibited a higher sensitivity than the CNT-FET biosensor with a chemical linker. In addition, we found that *E. coli* OM with autodisplayed Z-domains of protein A provided a higher sensitivity and a more effective blocking of the unspecific binding in comparison with protein G, which was possibly ascribed to the highly negatively charged *E. coli* OM (Jose et al., 2009, 2010).

Finally, we have applied the CNT-MESFET biosensors modified with *E. coli* OM with autodisplayed Z-domains to the detection of amyloid-β (Aβ) in human serum, a biomarker for early diagnosis of Alzheimer's disease. Although measuring Aβ levels in cerebrospinal fluid (CSF) is now considered to be useful for predicting the severity and progression of the disease, the lumbar puncture to obtain CSF is a more invasive procedure than blood sampling and thus has a critical limitation for repeat testing (Schneider et al., 2009). Additionally, plasma Aβ levels are much lower than CSF Aβ levels (Schneider et al., 2009); therefore ultra-high sensitive biosensors would be required to measure Aβ in human serum and provide reliable test-retest data. Aβ has been usually measured using enzyme-linked immune sorbent assay (ELISA); however, the sensitivity of ELISA is not high enough to detect Aβ in biological fluids at levels below 10 pg/mL (Fagan et al., 2009; Schupf et al., 2008). In addition, several label-free biosensors, such as STM-based (Kang et al., 2009) or reduced grapheme oxide-based biosensor (Kurkina et al., 2012), were reported to measure Aβ in PBS. Although they exhibited ultra-high sensitivity, Aβ in biological fluids was not measured, limiting their practical applications. In contrast, our CNT-MESFET biosensors permitted the real time detection of Aβ at levels as low as 1 pg/mL in human serum. These results suggest that CNT-MESFET biosensors with the protein engineered membrane containing Z domain might be a promising tool for identifying the role of serum Aβ as a biological marker for the early diagnosis of Alzheimer's disease.

2. Materials and methods

2.1. Materials

Polyclonal anti-horseradish peroxidase (HRP, antibody), purified HRP and anti-mouse (goat polyclonal) antibodies conjugated with 20 nm gold nanoparticles were purchased from Abcam (Cambridge, UK). Amyloid-β antibody (Santa Cruz Biotechnology, Santa Cruz, CA, USA), amyloid-β (1-42, human) (GL Biochem (Shanghai) Ltd., Shanghai, China) and Cys-3 protein G (Bioprogen, Deajeon, Korea) were commercially obtained. Bovine serum albumin (BSA), 3-aminopropyltriethoxysilane (APTES) and 1-pyrenebutanoic acid succinimidyl ester (chemical linker) were bought from Sigma-Aldrich Korea (Seoul, Korea). The 1 × phosphate buffered saline (PBS; pH) was purchased from AMRESCO® and composed of 137 mM NaCl, 2.7 mM KCl, and 10 mM phosphate buffer in 500 mL distilled H_2O. Separated semiconducting enriched single walled carbon nanotubes (SWNTs; 99%) were purchased from NanoIntegris Inc. (Skokie, IL, USA), whose diameter and length were 0.8–1.2 nm and 0.1–1 μm, respectively.

2.2. Fabrication of CNT-FET and CNT-MESFET

A uniform CNT film was prepared on an amine terminated Si/SiO_2 substrate by dropping a solution of separated semiconducting SWNTs in deionized water at 2% weight per volume (w/v) surfactant, sodium dodecyl sulfate (Kim et al., 2011). After leaving for 1 h, the specimen was rinsed with deionized water and dried with N_2 gas. Source (S) and drain (D) (Au (50 nm)/Cr (3 nm)) electrodes were patterned by conventional photolithography and lift-off techniques, followed by rapid thermal annealing at 450 °C for 30 s in a vacuum to form good contacts. Then, CNT channels with a width of 10 μm and a length of 5 μm were defined by an electron beam lithography technique with a negative resist (AR-N-7500, Allresist GmbH, Germany) and then unwanted CNTs were removed using O_2 plasma (Fig. 1(d)). The fabricated CNT-FET devices were characterized by measuring the I_{SD}–V_{SD} and I_{SD}–V_{BG} curves with a semiconductor parameter analyzer (Keithley 4200-SCS). After that, the top gate was fabricated by depositing Au (10 nm) only on the middle of the semiconducting CNT channel to construct CNT-MESFET devices (Fig. 1(e)). Finally, the source/drain electrodes and the CNT parts uncovered by the top gate were passivated by depositing a SiO_2 thin film, leaving only the Au top gate, and then a PDMS well was mounted over the CNT-MESFET.

2.3. Fabrication of E. coli OM with autodisplayed Z-domains of protein A

The autodisplay was performed by transformation using an autodisplay vector constructed by the cloning of the antibody binding Z-domain from *Staphylococcus aureus*, as described in the previous work (Jose et al., 2009, 2010). The OM of *E. coli* with autodisplayed Z-domain was also prepared by using lysozyme reaction and subsequent isolation procedures, as previously reported (Jose et al., 2009, 2010). The OM of intact *E. coli* was also prepared by

the same procedure. The OM solution was prepared having a total protein concentration of 300 μg/mL in PBS. For the coating of sensor surface, 100 μL of the OM solution was incubated for 2 h at room temperature. Then, the sensor surface was washed with 0.1% Tween 20 in PBS for three times. To immobilize the detection antibodies, the corresponding antibody solution (100 μL) was dispensed at the sensor surface and then incubated for 2 h at room temperature.

2.4. Real-time detection of analytes

To detect analytes, 20 μL of HRP or amyloid-β solution were added into the PDMS well and the electrical conductance was measured with a semiconductor characterization system (Keithley 4200-SCS). Human serum used in our studies was obtained from a repository for biofluids of patients, which had been gathered in a memory clinic through informed consents under an approval of Institutional Review Board. Originally, whole bloods were collected in BD Vacutainer serum separation tube (BD Biosciences, San Jose, CA, USA) and centrifuged at 3000 rpm for 5 min. Then, supernatant serum was transferred into Eppendorf tubes and stored in a deep freezer at −80 °C before use.

3. Results and discussion

A high density CNT film was prepared on an amine terminated Si/SiO_2 substrate by dropping a solution of separated semiconducting-enriched single walled CNTs (Fig. 1(b)). Source (S) and drain (D) electrodes were made by depositing Cr (3 nm)/Au (50 nm) (Fig. 1(c)). Then, the channels with a width of 6 μm and a length of 10 μm were defined by an electron beam lithography technique with the negative resist and the CNTs outside the channel region were removed using oxygen plasma ashing, resulting in CNT-FET devices (Fig. 1(d)). The thickness of CNT film measured by an atomic force microscope was 2–3 nm. In order to form good contacts, the devices were annealed at 450 °C for 30 s in vacuum, and then characterized by measuring source-drain current (I_{SD})–backgate voltage (V_{BG}) transfer curves under ambient conditions, where the heavily doped Si substrate was used as a bottom gate. Almost all devices exhibited a p-type semiconducting behavior, and similar values of on/off ratio and V_{th} were found: average values of on/off ratio and V_{th} were approximately $8.8 \times 10^4 \pm 4.7 \times 10^4$ and 0.37 ± 0.31 V, respectively (Fig. S2). These results implied that the prepared films were quite uniform and mostly composed of semiconducting CNTs. After that, Au top gates were deposited only at the middle of the CNT channel to fabricate CNT-MESFET (Fig. 1(e)). The I_{SD}–V_{BG} transfer curve under ambient conditions obtained from the CNT-MESFET is shown in Fig. 2(a). As for the CNT-FET, the p-type semiconducting behavior was observed for almost all CNT-MESFET devices, although the V_{th} was shifted to the higher V_{BG}.

Most biological interactions occur under aqueous conditions, so biosensors usually operate in an aqueous environment. Hence, the source/drain electrodes and the CNT parts uncovered by the top gate were passivated by depositing a SiO_2 thin film, followed by mounting a polydimethylsiloxane (PDMS) well over the CNT-MESFET. Fig. 2(b) shows the I_{SD}–V_{BG} transfer curves measured with PBS in the PDMS well. Interestingly, a significant decrease in subthreshold swing defined as $S = dV_{BG}/d(\log I_{SD})$ was observed. The value of S was estimated to be about 1.3 and 3.0 V/decade under ambient conditions for CNT-FET and CNT-MESFET, respectively (inset of Fig. 2(a)). However, the value of S decreased to about 0.4 and 0.18 V/decade under aqueous conditions for CNT-FET and CNT-MESFET, respectively (inset of Fig. 2(b)). Since there is a reciprocal relation between S and a gate capacitance (Sze, 1981), these findings suggested that the gate capacitance in the liquid condition was larger than the gate capacitance under ambient conditions. In the ambient conditions, the CNT channel was influenced by V_{BG} only through the SiO_2 layer. Under aqueous conditions, however, the CNT channel was probably affected by V_{BG} via the SiO_2 layer as well as by PBS since the double layer capacitance, $C_{dl} = \varepsilon A/x_{OHP}$, in the aqueous condition is not negligible; ε is the dielectric constant of the electrolyte, A is the area of the surface exposed to the electrolyte, x_{OHP} is the distance to the outer Helmholtz plane (Bard and Faulkner, 2001; Heller et al., 2006). Consequently, the gate capacitance might be larger under aqueous conditions than in ambient conditions, leading to the smaller S in the aqueous environment. Furthermore, since the CNT-MESFET had a larger A than the CNT-FET, the smaller S observed with the CNT-MESFET under aqueous conditions might be attributed to the larger C_{dl} of the CNT-MESFET.

To characterize the CNT-MESFET biosensor, we immobilized anti-HRP antibodies on the Au top gate surface of CNT-MESFET

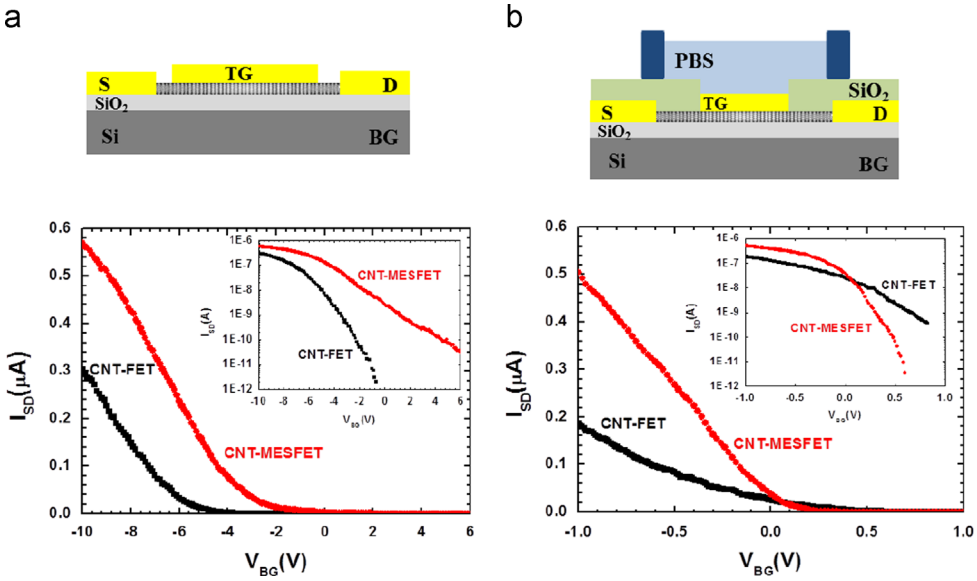

Fig. 2. I_{SD}–V_{BG} transfer curves measured at V_{SD}=1 V in (a) ambient conditions and (b) aqueous conditions for CNT-FET (black symbols) and CNT-MESFET (red symbols). The insets show the I_{SD}–V_{BG} transfer curves on the semi-logarithm scale. (For interpretation of the references to color in this figure legend, the reader is referred to the web version of this article.)

using protein G (MESFET-G, Fig. 3(a)) or *E. coli* OM with auto-displayed Z-domains of protein A (MESFET-Z, Fig. 3(b)). For comparison, we also prepared a CNT-FET based biosensor with anti-HRP antibodies immobilized on the surface of the CNTs using pyrenebutyric acid *N*-hydroxylsuccinimide ester (FET-C, Fig. 3(c)). The I_{SD}–V_{BG} transfer curves measured before and after detection of HRP are shown in Fig. S3(a, b, and c) for MESFET-G, MESFET-Z, and FET-C, respectively. After binding of HRP to anti-HRP antibodies, V_{th} shifted to the positive V_{BG} for all sensors, leading to an increase in the conductance at $V_{BG}=0$ V.

The real-time conductance was measured for MESFET-G, MESFET-Z, and FET-C while different concentrations of HRP in PBS were added in the PDMS well (Fig. 3(d)). Binding of HRP to anti-HRP antibodies caused an increase in conductance for all sensors (Fig. S3(a, b, and c)), although the increasing rates of the conductance differed depending on the sensor. Compared to FET-C, MESFET-Z or MESFET-G exhibited a more rapid increase in conductance as the HRP concentration increased. For MESFET-G and MESFET-Z, the potential of the CNT channel covered with the Au top gate was affected by binding of HRP to anti-HRP antibodies, while the potential of the uncovered CNT portion was unchanged. As a result, energy bending might be induced within the CNT, resulting in the larger conductance change for MESFET-G or MESFET-Z than for FET-C (Oh et al., 2010). Moreover, as the HRP concentration rose, the conductance of MESFET-Z increased more rapidly than the conductance of MESFET-G. These observations indicated that the sensitivity of MESFET-G or MESFET-Z was higher than that of FET-C, and that of MESFET-Z exceeded that of MESFET-G.

Fig. 3(e) depicts the plot of the conductance change normalized by the initial conductance ($\Delta G/G_0$) versus HRP concentration in a logarithmic scale for MESFET-Z, MESFET-G, and FET-C. Data were measured using three independent sensors and then averaged. As expected from Fig. 3(d), the steepest slope was observed for MESFET-Z, although a linear relationship was observed in the range of 10^{-12}–10^{-9} g/mL of HRP and the limit of detection estimated by assuming 3.3 × standard deviations was approximately 10^{-13} g/mL for all sensors. It was also noted that the standard deviations were relatively small, suggesting that the device-to-device variation was significantly reduced.

To investigate why the MESFET-Z exhibited higher sensitivity than the MESFET-G, we immobilized the antibodies conjugated with 20 nm-diameter Au nanoparticles on MESFET-Z or MESFET-G and obtained field emission electron microscopy (FESEM) images (Fig. 4). More Au nanoparticles were found in MESFET-Z than in MESFET-G, suggesting that more antibodies were immobilized on the Au surface with protein engineered membrane containing Z domain than with protein G, accounting for the higher sensitivity of MESFET-Z. Similar experiments were also carried out for FET-C (Fig. 4(c)). FET-C showed a lower density of Au nanoparticles in comparison to MESFET-G, which was consistent with the measured real-time conductance (Fig. 3(d and e)).

For clinical application of biosensors, target analytes in blood or serum must be detected in the presence of various other endogenous proteins. Thus, we also measured $\Delta G/G_0$ for different concentrations of HRP in human serum using MESFET-Z or MESFET-G (Fig. 5(a)). In the case of MESFET-Z, the plot of $\Delta G/G_0$ versus log(HRP concentration) showed similar slopes for HRP in serum and PBS. On the other hand, in studies with MESFET-G, we observed some deviations in the plots, which were probably due to the nonspecific binding. These results implied that the nonspecific binding was much more effectively blocked for MESFET-Z than for MESFET-G. Since the Zeta potential measured with dynamic light scattering (DLS, Zetasizer Nano ZS, Malvem Instruments Ltd.) was about −33.9 mV and −18.6 mV for *E. coli* OM and protein G, respectively, the effective blocking of nonspecific binding for MESFET-Z was attributable to the highly negatively charged *E. coli* OM (Jose et al., 2010). Fig. 5(b) shows $\Delta G/G_0$ of MESFET-Z in

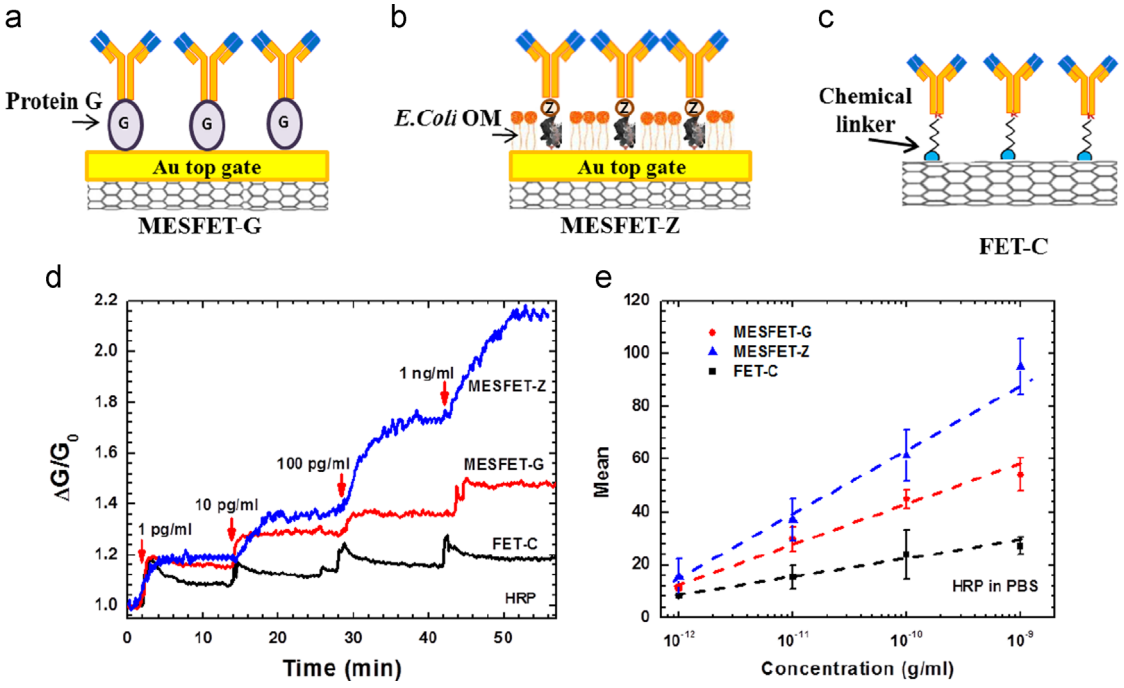

Fig. 3. Schematic diagrams of (a) MESFET-G, (b) MESFET-Z, and (c) FET-C. Each molecule was assembled successively from bottom to top. (d) Real time monitoring of $\Delta G/G_0$ measured for FET-C (black symbols), MESFET-G (red symbols), and MESFET-Z (blue symbols) while different concentrations of HRP in PBS were added. (e) $\Delta G/G_0$ versus concentration of HRP in PBS on the semi-logarithm scale for FET-C (black symbols), MESFET-G (red symbols), and MESFET-Z (blue symbols). Data represent mean ± standard deviation ($n=3$). The calibration lines are fitted to $\Delta G/G_0=(6.53\pm0.79)$ log(concentration) ± 87.26 for FET-C, $\Delta G/G_0=(14.47\pm1.47)$ log(concentration) ± 186.90 for MESFET-G, and $\Delta G/G_0=(22.9\pm0.92)$ log(concentration) ± 209.23 for MESFET-Z. (For interpretation of the references to color in this figure legend, the reader is referred to the web version of this article.)

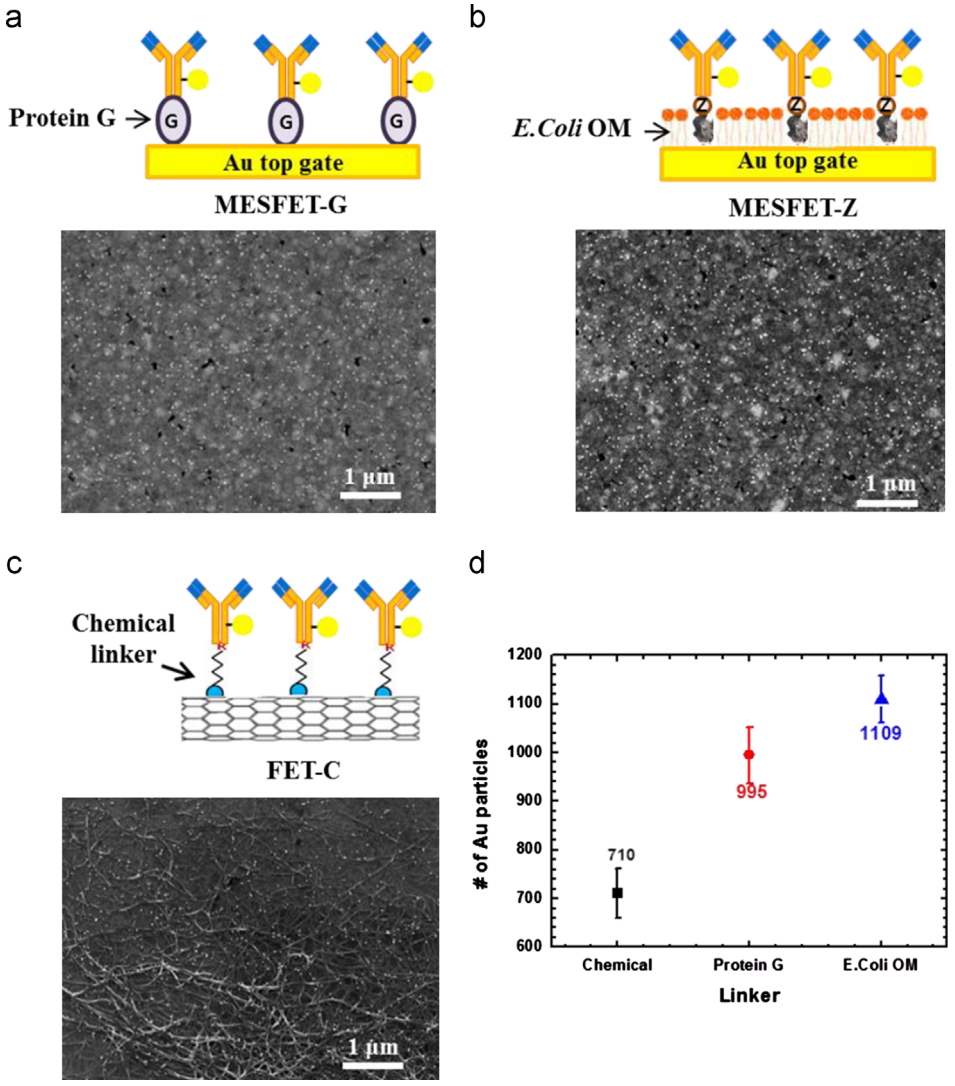

Fig. 4. FESEM images of antibodies conjugated with 20 nm-diameter Au nanoparticles on (a) MESFET-G, (b) MESFET-Z, and (c) FET-C. (d) The number of Au nanoparticles immobilized in the area of $200 \times 200\ \mu m^2$ using protein G, *E. coli* OM with autodisplayed Z-domains of protein A, or chemical linker. Data represent mean ± standard deviation ($n=3$).

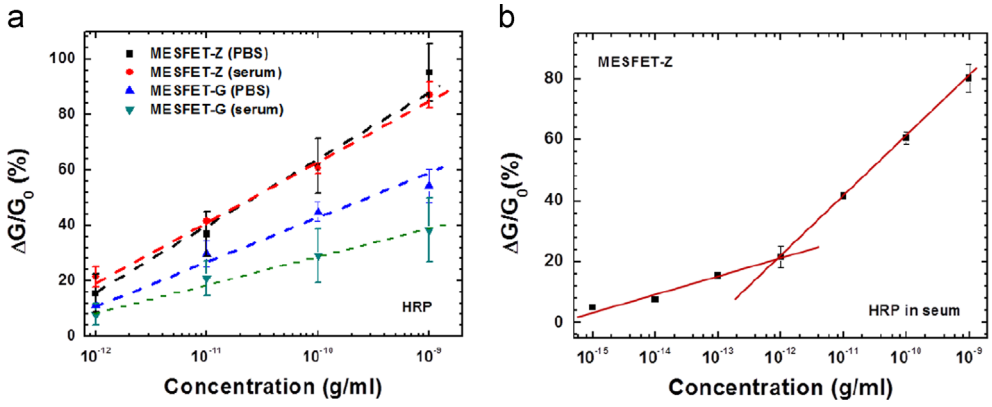

Fig. 5. (a) Real time monitoring of $\Delta G/G_0$ measured for MESFET-G and MESFET-Z upon the addition of different concentrations of HRP in PBS or human serum. (b) $\Delta G/G_0$ versus concentration of HRP in human on a semi-logarithm scale for MESFET-Z. Data represent mean ± standard deviation ($n=3$).

the range of 1×10^{-15}–1×10^{-9} g/mL of HRP in serum. Although different slopes were observed below and above 1×10^{-12} g/mL of HRP, the concentration of 1×10^{-15} /mL caused $\Delta G/G_0 \approx 5\%$, meaning that the concentration lower than 1 fg/mL might be detected using MESFET-Z.

In addition to HRP, we also measured Aβ in human serum using MESFET-Z to determine whether MESFET-Z may be applied for the early diagnosis of Alzheimer's disease. As with HRP, the V_{th} shifted to the higher V_{BG} after binding of Aβ to Aβ antibodies (Fig. S4), and the conductance of MESFET-Z increased as the concentration of Aβ

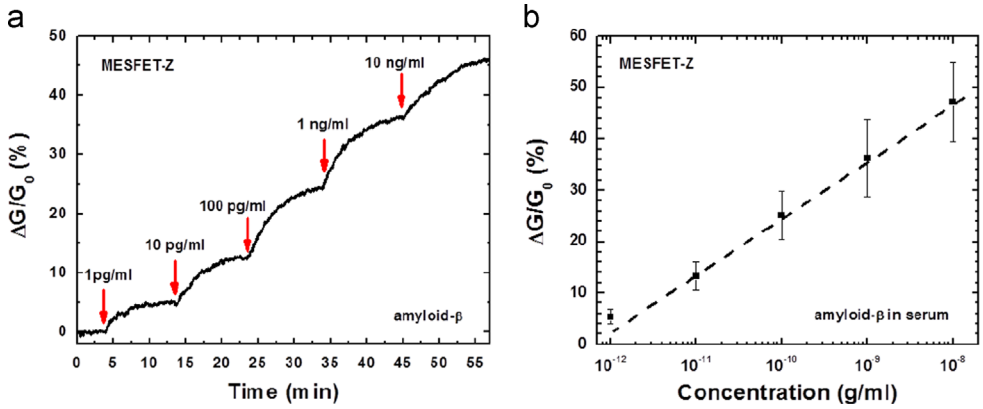

Fig. 6. (a) Real time monitoring of $\Delta G/G_0$ measured using MESFET-Z while different concentrations of amyloid-β in human serum were added. (b) $\Delta G/G_0$ versus concentration of amyloid-β in human measured using the MESFET-Z. Data represent mean ± standard deviation ($n=5$). The calibration line is fitted to $\Delta G/G_0=(10.64 \pm 0.38)$ log(concentration)+131.79.

increased (Fig. 6(a)). The plot of $\Delta G/G_0$ versus log(concentration) also revealed the linear relationship in the range of 10^{-12}–10^{-9} g/mL of Aβ in serum, although its slope was somewhat slower that for HRP (Fig. 6(b)). For Aβ of 1 pg/mL in serum, $\Delta G/G_0 \approx 5.4\%$ was measured, implying that Aβ lower than 1 pg/mL may be detected. These results demonstrated that MESFET-Z might be used to detect Aβ in clinical samples in real-time and without labeling.

4. Conclusion

We have explored the CNT film-based IA biosensor with the metal semiconductor field effect transistor structure by depositing a Au top gate on the middle of the CNT channel. In order to detect HRP used as the model analyte, anti-HRP antibodies were immobilized on the Au top gate with protein G or autodisplayed Z-domains of protein A as the antibody-binding protein. Compared to the CNT-FET biosensors where probe antibodies were immobilized on the sensor surface using a chemical linker, CNT-MESFET biosensors were more highly sensitive since the density of probe antibodies with the proper orientation immobilized on the sensor surface was enhanced by using antibody-binding proteins. Moreover, for MESFET-Z, nonspecific binding was well inhibited because of the highly negatively charged *E. coli* OM, so HRP at levels as low as 1 fg/mL in serum could be measured using MESFET-Z. Finally, we applied the MESFET-Z to the detection of amyloid-β in human serum, which is one of the biomarkers related to Alzheimer's disease. Aβ at the level of 1 pg/mL in human serum could be detected using MESFET-Z and a linear relationship was observed in the plot of conductance change versus concentration on the semi-logarithm scale for the range of 10^{-12}–10^{-9} g/mL. These results demonstrated a possible application of the MESFET-Z to the real-time detection of Aβ in blood samples.

Acknowledgments

This work was financially supported by MEST through the National Research Foundation (NRF) of Korea (Nos. 2011-0017486 and 2012R1A102906). This work was supported by the Yonsei University Research Fund of 2012.

Appendix A. Supporting information

Supplementary data associated with this article can be found in the online version at http://dx.doi.org/10.1016/j.bios.2013.07.004.

References

Allen, B.L., Kichambare, P.D., Star, A., 2007. Advanced Materials 19, 1439–1451.
Bard, A.J., Faulkner, L.R., 2001. Electrochemical Methods: Fundamentals and Applications, second ed. Wiley, New York.
Chen, R.J., Zhang, Y., Wang, D., Dai, H., 2001. Journal of the American Chemical Society 123, 3838–3839.
Fagan, A.M., Head, D., Shah, A.R., Marcus, D., Mintun, M., Morris, J.C., Holtzman, D.M., 2009. Annals of Neurology 65, 176–183.
Heller, I., Kong, J., Williams, K.A., Dekker, C., Lemay, S.G., 2006. Journal of the American Chemical Society 128, 7353–7359.
Hu, P., Zhang, J., Wen, Z., Zhang, C., 2011. Nanotechnology 22, 335502.
Jose, J., Chung, J.W., Jeon, B.J., Maasa, R.M., Nam, C.H., Pyun, J.C., 2009. Biosensors and Bioelectronics 24, 1324–1329.
Jose, J., Park, M., Pyun, J.C., 2010. Biosensors and Bioelectronics 25, 1225–1228.
Kang, D.-Y., Lee, J.-H., Oh, B.-K., Choi, J.-W., 2009. Biosensors and Bioelectronics 24, 1431–1436.
Kim, H.J., Hwang, S., Oh, J., Chang, Y.W., Lim, E.K., Haam, S., Kim, C.S., Yoo, K.-H., 2011. Nanotechnology 22, 045703.
Kurkina, T., Sundaram, S., Sundaram, R.S., Re, F., Masserini, M., Kern, K., Balasubramanian, K., 2012. ACS Nano 6, 5514–5520.
Li, C., Curreli, M., Lin, H., Lei, B., Ishikawa, F.N., Datar, R., Cote, R.J., Thompson, M.E., Zhou, C.W., 2005. Journal of the American Chemical Society 127, 12484–12485.
Maehashi, K., Katsura, T., Kerman, K., Takamura, Y., Matsumoto, K., Tamiya, E., 2007. Analyitcal Chemistry 79, 782–787.
Oh, J., Yoo, S., Chang, Y.W., Lim, K., Yoo, K.H., 2009. Current Applied Physics 9, e229–e231.
Oh, J., Chang, Y.W., Kim, H.J., Yoo, S., Kim, D.J., Im, S., Park, Y.J., Kim, D., Yoo, K.H., 2010. Nano Letters 10, 2755–2760.
Schneider, P., Hampel, H., Buerger, K., 2009. CNS Neuroscience & Therapeutics 15, 358–374.
Schupf, N., Tang, M.X., Fukuyama, H., Manly, J., Andrews, H., Mehta, P., Ravetch, J., Mayeux, R., 2008. Proceedings of the National Academy of Sciences of the United States of America 105, 14052–14057.
Sze, S.M., 1981. Physics of Semiconductor Devices, second ed. Wiley, New York.
Wang, C., Zhang, J., Ryu, K., Badmaev, A., Arco, L.G.D., Zhou, C., 2009. Nano Letters 9, 4285–4291.